Non-Intrusive Device for Real-Time Circulatory System Assessment with Advanced Signal Processing Capabilities

E. Pinheiro, O. Postolache, P. Girão

Instituto de Telecomunicações, Instituto Superior Técnico, Av. Rovisco Pais 1, 1049-001, Lisboa, Portugal,
eduardo.pinheiro@lx.it.pt, opostolache@lx.it.pt, p.girao@lx.it.pt

This paper presents a device that uses three cardiography signals to characterize several important parameters of a subject's circulatory system. Using electrocardiogram, finger photoplethysmogram, and ballistocardiogram, three heart rate estimates are acquired from beat-to-beat time interval extraction. Furthermore, pre-ejection period, pulse transit time (PTT), and pulse arrival time (PAT) are computed, and their long-term evolution is analyzed. The system estimates heart rate variability (HRV) and blood pressure variability (BPV) from the heart rate and PAT time series, to infer the activity of the cardiac autonomic system. The software component of the device evaluates the frequency content of HRV and BPV, and also their fractal dimension and entropy, thus providing a detailed analysis of the time series' regularity and complexity evolution, to allow personalized subject evaluation.

Keywords: Biomedical instrumentation, blood pressure, cardiovascular system, heart rate, medical services, time series

1. INTRODUCTION

NON-INVASIVE cardiovascular system assessment is generally done using electrophysiological signals, such as the electrocardiogram (ECG) or the photo-plethysmogram (PPG), to estimate heart rate and oxygen saturation. In addition to the morphological properties of these signals, timing aspects are of utmost importance, as the heart rate gives information on several physical and mental stresses, emergency situations and also on neural control of the heart [1].

The heart rate may be determined from any biological signal with the same periodicity of the cardiac cycle, provided that enough accuracy in periodicity detection is guaranteed. The progresses in the study of heart rate lead to the discovery of two important markers of the autonomic cardiovascular regulation: heart rate variability (HRV), and blood pressure variability (BPV) [2].

HRV analyzes how cardiac cycle period varies and it is accepted as a diagnostic tool, in view of the fact that several pathologies change the cardiovascular control mechanisms [1]-[4] and HRV reflects maladies associated with sympathetic and parasympathetic branches of the autonomic nervous system [1], [5]-[6]. HRV and BPV are able to forecast cardiovascular risks [4]-[7], hence precise measurement of these parameters is required to avoid false diagnosis.

BPV is linked to amplitude variations of blood pressure, but recent works have tried to assess blood pressure (BP) without the use of direct measurement devices. Indirect time-based measurements, such as the pulse arrival time (PAT) or the pulse transit time (PTT), have been applied with positive results. The existence of a significant correlation between the variabilities of PAT and BP [8]-[17] has been established. Even systolic blood pressure may be estimated from PAT, requiring calibration to a number of patient's physiologic characteristics [18].

When evaluating the cardiac function, the patient's stress acts as an important bias source, as involuntary psychophysiological responses related to the measurements'

stress affect both the heart rate and blood pressure [2]. It is important to reduce invasiveness and the occupation of the patient's comfort space by the measurement apparatus. The device presented here implements the ballistocardiogram (BCG), ECG, and PPG sensors. By integrating chair seat BCG and finger PPG transducers, the obtrusiveness of the cardiac evaluation tests is diminished. In the least obtrusive scenario ECG would be replaced by BCG, thus avoiding the usage of electrodes, and having the patient comfortable during the measurements, at the cost of loosing information related to the electrical stimulus to the myocardium. PTT evaluation may be done solely with BCG and PPG. The ECG was included to provide a third estimate of HRV, to assess the estimates provided by the other signals, and because it allows measurements of pre-ejection period (PEP) and PAT.

Fractal dimension and entropy-based methods have been used in cardiology in the last years and have derived important conclusions in HRV analysis [19]-[27]. In the present case, they were applied to HRV and to PAT and PTT variabilities (PATV, PTTV). The proposed device allows gathering a substantial amount of data, with subject's minimal discomfort, and characterizes the fractal dimension, Shannon, Rényi and Tsallis entropies of the subject's HRV and BPV.

Variability monitoring requires some recording time to compile sufficient data for the analysis to be meaningful. The unobtrusive sensors, namely BCG, are very useful as they reduce the patient's annoyance with the measurement process. After some minutes of recording it is possible to assess deviations on the subject's regular HRV parameters. Changes in the autonomic system and some modifications in the patient's contractile mechanism may be signalized by these methods [2],[4],[5],[19]-[22]. A group of healthy subjects experimented with the system, in order to provide validation data to evaluate the system's cardiovascular monitoring ability.

Subsequently, the paper gives details of the design, realization, and validation of the device's hardware and software components. The hardware component that regards

the sensors and signal conditioning circuitry acquiring BCG, ECG, and PPG, is presented in section 3. The software component that regards the device capabilities to interact with the user and to analyze the gathered data, is presented in section 4. The results validating the device based on a healthy test group, the discussion of the results, and the respective conclusions compose sections 5 and 6 of the paper.

2. DEFINING CONCEPTS

A. Cardiovascular delays

The time difference between the ECG R-wave and the PPG foot is usually named pulse arrival time. This delay is also referred to in literature as pulse wave transit time, pulse wave delay or also pulse wave velocity, [9]-[14]. Recent literature reports the existence of a significant correlation between PATV and BPV [8]-[17], showing, in particular, that the most relevant correlation is obtained when defining PAT as the R-wave to PPG foot delay [11]. Accordingly, the measurement of PAT under this definition will improve the characterization of the patient's cardiovascular status.

Although being used in current applications to estimate BP [12],[16],[18], the exactness of PAT application for this purpose is argued [28],[29]. A subject-dependent BP-PAT relation, (1), has been presented earlier [18]. Using it, the device may obtain not only BPV but also systolic BP, SBP, though being unable to estimate diastolic BP. The constants b and k are obtained by calibration, L is the length of each subject's right arm, and d is the density of the subject's blood (e.g. 78 cm and 1060 kg/m^3).

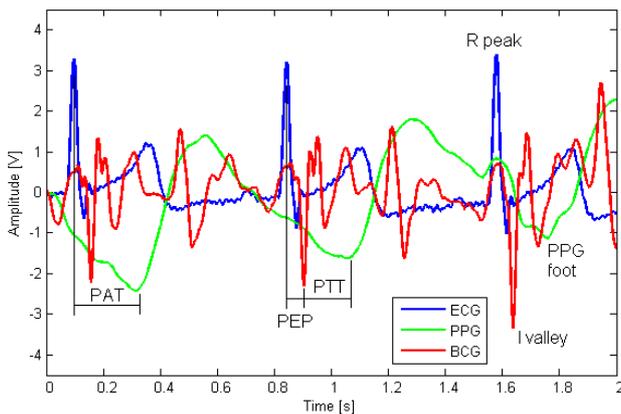$$ SBP = \frac{1}{b} \ln\left(\frac{L^2 db}{(PAT - k)^2} - 1 \right) \qquad (1) $$

Fig.1. The three signals acquired by the system, with the most important parameters marked.

The PEP is the duration of electro-mechanical delay plus the isovolumetric ventricle contraction up to the aortic valve opening and it is a variable additive delay, which changes rapidly in response to stress, emotion and physical effort [30]. The use of PAT instead of PTT improves the correlation with systolic BP [31]. The use of PTT is justified by the unobtrusiveness of its acquisition. PAT is better in

isolating the effects of administration of different vasoactive drugs [31], and also when inducing physical stress in normal subjects [30]. In spite of this shortcoming, it is profitable to measure PTT using BCG and PPG, as it will not induce stress in the subject and it will still be possible to estimate SBP. To evaluate PEP or PAT the ECG must be acquired, while PTT measurement only requires unobtrusive measurements.

Our recent work underline the relation between PAT and PTT, for a group of healthy subjects, using the I valley of the BCG as reference for PTT evaluation [17]. Fig.1 shows 2 seconds of BCG, ECG and PPG acquired with the developed device, where the synchronism of the most prominent waves of each signal is evident.

Since the I valley of the BCG marks the start of ejection, being related to the acceleration of blood into the pulmonary artery and ascending arch of the aorta [32], it is appropriate for dividing the PAT into the PEP and the PTT components. This enables a more detailed analysis on the subject's condition by discriminating the purely vascular component, PTT, from the ejection delay component, PEP.

It is of particular interest to analyze the long-term evolution of the parameters gathered. To express in detail information on the evolution of the cardiovascular parameters, several information measures are taken.

B. Fractal and complexity measures

Fractal dimension analysis of an HRV time series has been presented as an effective measurement of autonomic nervous system response [20]-[21]. The fractal dimension computed by the device is the Minkowski-Boulingand dimension.

For HRV, a fractal set, with Minkowski-Boulingand dimension D_{MB} and area $A(r)$ traced by a circle of radius r along the fractal, allows to write $\frac{A(r)}{2r} = kr^{1-D_{MB}}$, therefore conducing to the limit presented in (2), formal definition of the Minkowski-Bouligand dimension [33].

$$ D_{MB} = \lim_{r \to 0} \frac{\log A(r)}{\log(1/r)} + 2 \qquad (2) $$

$$ D_{HB} = \lim_{l \to 0} \frac{\log N(l)}{\log(1/l)} \qquad (3) $$

The preceding formulation of Minkowski-Bouligand dimension is remindful of the Hausdorff-Besicovitch dimension definition (3), with $A(r)$, the area of the circle with radius r, replacing $N(l)$ the number of line segments with length l, needed to cover the curve. These dimensions have a tight relation, and their values coincide for a number of known cases, but Minkowski-Bouligand dimension is easily computed.

The calculation of (2) was implemented in MATLAB and the script was embedded in the software. The Minkowski-Bouligand dimension is computed when new values of the HRV and BPV time series are available. For instance in Fig.4, the fractal dimension of the HRV time series obtained

from the ECG is the only one being computed, but when PPG is visible, the respective HRV series is analyzed. However, it should be noticed that the fractal dimension is only significant when a large number of heart rate values is available, justifying the interest in having unobtrusive sensors in the device.

From the information theory point of view, entropy is a measure of order in dynamical systems, a statistical complexity measurement [27]. Entropy-based techniques are routinely employed in analysis of medical data, namely cardiovascular time-series. In this case, the heart and the circulatory system that compose the dynamical system were scrutinized. Three distinct entropies were implemented, Shannon (4), Tsallis (5) and Rényi (6), given their distinct properties.

$$S_S[P] = -\sum_{j=1}^{N} p_j \ln p_j \qquad (4)$$

$$S_T(q,[P]) = \frac{1}{q-1} \sum_{j=1}^{N} \left[p_j - p_j^{\,q} \right] \qquad (5)$$

$$S_R(\alpha,[P]) = \frac{1}{1-\alpha} \ln \left[\sum_{j=1}^{N} p_j^{\,\alpha} \right] \qquad (6)$$

$P \equiv \{p_1,...,p_N\}$ is the time series in consideration, q is the entropic index, and α the entropy order. Taking the limit $\alpha \to 1$, Rényi entropy coincides with Shannon entropy. The limit $q \to 1$ leads Tsallis entropy to coincide with the Shannon-Boltzmann-Gibbs entropy [24]. For the analysis of shorter and noisy time series, the Kolmogorov-Sinai entropy may be used to estimate the mean rate of creation of information [34]. With wide use in physiology and medicine, approximate entropy [35], and a modified algorithm, sample entropy [36], have been proposed.

Having some advantages, approximate and sample entropy, however, assign higher entropy to some pathologic time series that represent less complex dynamics than to time series derived from healthy cardiovascular dynamics [37]. Therefore, as the device is able to obtain long recordings, the entropies defined in (4), (5), and (6) were implemented instead. HRV is assessed by the use of three signals. PATV, PTTV, and PEPV are assessed by the measures (4)-(6). These computations diminish the uncertainty of the entropy estimation, and provide an accurate description of the cardiovascular system status. All these entropies are computed swiftly in real-time and calculated whenever the time series is updated.

3. DEVICE OVERVIEW - HARDWARE

The device hardware is composed of the respective sensors, with dedicated conditioning circuits, a multifunction data acquisition board (DAQ), NI 6024E, and a laptop PC which implements the data processing algorithms necessary to investigate the cardiovascular parameters. The sampling frequency used was 1.5 kHz so the digitalization will not affect the PATV correlation with BPV, as this sampling rate allows peak detection with an appropriate resolution [1]-[2].
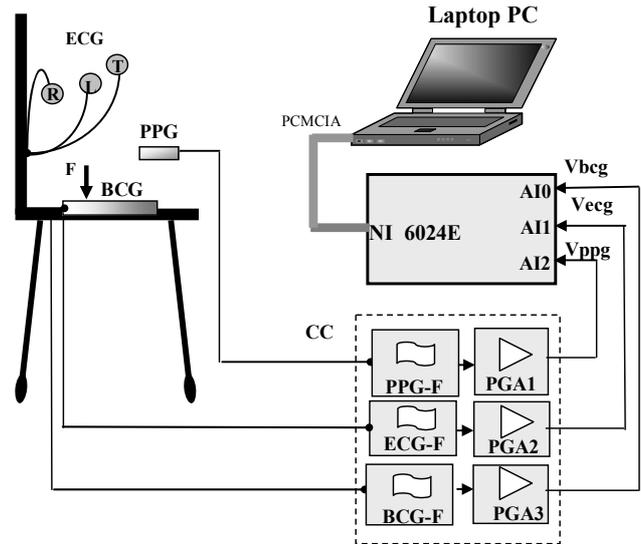

Fig.2. BCG, ECG and PPG measurement system (PGAi – programmable gain amplifiers, BCG-F – ballistocardiogram signal filter, PPG-F – plethysmography filter, ECG-F- electrocardiogram filter).

To acquire the BCG, an electromechanical film (EMFi) sensor was placed under the seat of a normal office chair, while the ECG was acquired using three chest leads and the PPG by evaluating index finger absorption of red light [8]. Fig.2 depicts the system.

A. Ballistocardiogram

The BCG acquisition is based on the unnoticeable implementation of an electromechanical film sensor (EMFIT L-series) inside an office chair's seat. The transducer is composed of exterior homogeneous surface layers having in its interior a number of thin polypropylene layers with air voids [38], generating a scarce electric charge variation at the sensors' electrodes.

The BCG signal is obtained connecting the EMFi output to a low-noise and high input impedance charge amplifier scheme based on a low-noise (50 nVHz$^{-1/2}$, at 10 Hz), high input impedance (10^{12} Ω ∥ 8 pF) TLC2274 operational amplifier. The charge amplifier gain is controlled by a 50 kΩ X9C503 digital potentiometer. In addition to the amplification stage, analog filtering is also implemented using an active 2nd order 150 Hz Butterworth low-pass filter to prevent aliasing, and a 0.05 Hz high pass filter of the same characteristics, to remove any trace of dc component. This cut-off frequency, whilst diminishing power line interference and high frequency noise, does not interfere with the signal's frequencies [39]. The BCG signal conditioning circuitry is connected to the analog input AI0 of the data acquisition board and is sampled at 1.5 kHz. After being acquired, the BCG is subject to a Kaiser window, with beta 0.5, FIR notch filter in order to obtain a clearer signal. The systolic and diastolic waves of the BCG are visible, as well as a prominent I valley, see Fig.1.

An adaptive peak detector was built using LabVIEW peak detection functions [8], capable of adapting itself to the patient's peak amplitude and using spline interpolation, to determine the I valley position in the BCG signal. The heart

rate is computed from the delay between consecutive I valleys obtained from the peak detection processing block output.

B. Electrocardiogram

The ECG acquisition circuitry was developed for a three lead scheme. Three standard patch-type ECG electrodes were placed on the subject's chest in a triangular disposition to respect the Einthoven triangle.

The gathered electromotive force is applied to the inputs of an instrumentation amplifier scheme based on INA118, an integrated circuit with low bias current (5 nA) and high common mode rejection ratio (110 dB), whose gain is controlled by an external resistor, another 50 kΩ X9C503 digital potentiometer. Afterwards, filtering stages remove baseline wandering and artifacts originating from subject movement or muscular activity. The signal was limited to a band of 0.05-150 Hz by the use of 2nd order high-pass and low-pass Butterworth filters implemented with TLC2274. The ECG signal conditioning output is connected to analog input AI1 of the DAQ. Power line interference was filtered by a FIR digital 50 Hz notch filter implemented in the LabVIEW signal processing block.

To determine the time stamp position of the QRS complex, the adaptive peak detector used for the BCG signal is used also for the ECG to find the R peak.

C. Photoplethysmogram

A finger PPG sensor has been developed. Its sensing principle is based on controlled red light emission by a LED and detection by a photodiode. The light transducer implemented is the photodiode TAOS TSL257. This sensor has an integrated transimpedance amplifier and is characterized by a high responsiveness in the red part of the electromagnetic spectrum (1.68 V/(μW/cm^2) at 645 nm). In comparison to a previous application of infrared light [8] where good results were obtained, improvements in the PPG signal quality were registered due to the better characteristics of the sensor used.

Using TLC2274 high-performance operational amplifiers, the transducer signal is amplified and limited to a maximum frequency of 150 Hz, its dc component is removed by the abovementioned 0.05 Hz high pass filter, and it is then acquired by the DAQ board analog input AI2. A FIR digital notch filtering is also employed to reduce power line traces in the PPG signal. The peak detector is used to identify the maximum peaks and the foot of the PPG waveform. The heart rate and the HRV are calculated based on beat-to-beat analysis.

4. DEVICE OVERVIEW - SOFTWARE

The software component of the device was developed in LabVIEW 8.6 with embedded MATLAB scripts. An informative graphical user interface (GUI), depicted in Fig.4 and Fig.5, and additional data-logging capabilities were implemented. Files with the most relevant parameters and raw data may be saved and analyzed offline using the data processing block of the software in order to evaluate trends and identify normal and abnormal situations.

A. Acquired signals

The BCG, ECG and PPG signals acquired with the DAQ board are subject to an initial analog filtering stage, afterwards a digital notch filter, and only then analyzed. The analog filters had a pass-band with maximally flat magnitude, and in the digital stage, a Kaiser window, with beta 0.5, FIR notch filter was used. All the channels present the same frequency response, shown in Fig.3, thus relative distortion between signals is minimized.
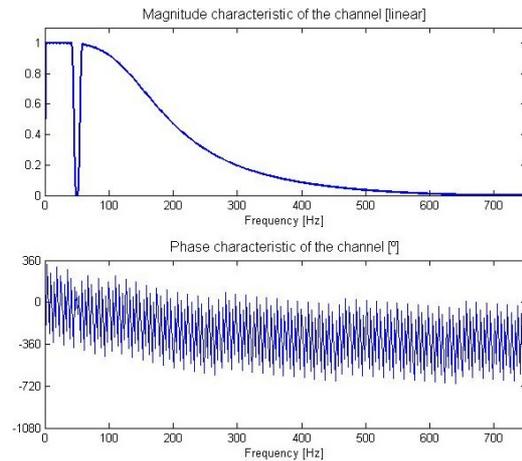

Fig.3. Frequency response of the combined analog (2nd order Butterworth 0.05-150 Hz) and digital (Kaiser window, beta 0.5, FIR notch filter) signal processing stages.
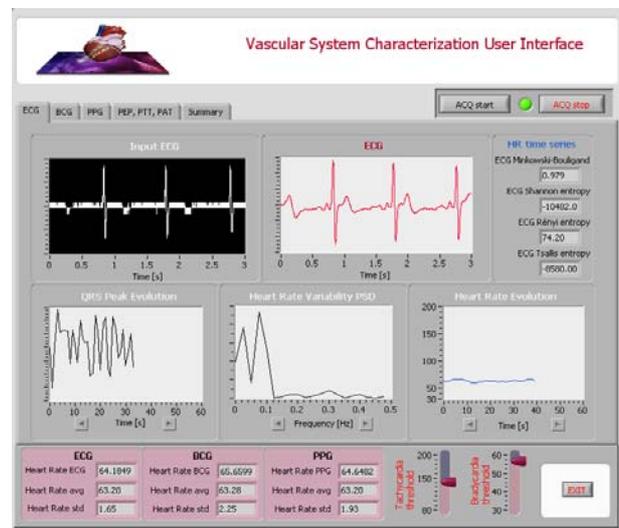

Fig.4. User interface "ECG" visualization mode after 39 seconds of recording. «Input ECG» is the raw signal acquired in the previous 3 seconds, contaminated with some powerline noise; «ECG» is the ECG signal gathered in the previous 3 seconds passed by the FIR notch filter; «QRS Peak Evolution» is the amplitude of the QRS peak, which depicts respiratory activity; «Heart Rate Variability PSD» is the power spectral density of the heart rate time series; «Heart Rate Evolution» shows the heart rate values calculated.

The information is presented to the user in separate windows for each of the acquired signals displaying: signal's main peak amplitude (QRS in the ECG, I valley in

the BCG, and main wave in the PPG); heart rate (instantaneous, long-term, average and standard deviation); HRV power spectral density (PSD), Minkowski-Bouligand dimension, Shannon, Rényi and Tsallis entropies. Alarm functions are also available, as tachycardia and bradycardia thresholds may be defined by the user, but by default are respectively 140 bpm and 56 bpm.

Fig.4 presents the GUI's "ECG" signal visualization window after 39 seconds of acquisition. It displays the QRS modulation by respiration (left), the estimate of the HRV PSD (center), and the previous stated complexity measures (top right), as well as the signals' heart rate estimates.

B. Cardiovascular parameters

The pre-ejection period is obtained from the delay between the ECG and the BCG main waves. The pulse transit time is obtained as the delay between the I valley of the BCG and the foot of the finger PPG. The pulse arrival time comes from the delay between the ECG QRS peak and the foot of the PPG. Similarly to the HRV processing, the PEP, PTT, and PAT power spectral density is also computed, to assess the autonomic function in the Very Low Frequency, Low Frequency, and High Frequency ranges [2]. Fig.5 displays the respective tab of the GUI, where the first row depicts the delays and the second their PSD.
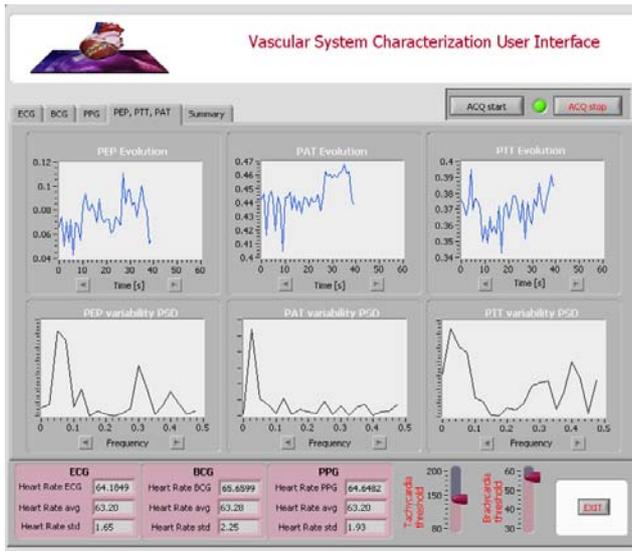

Fig.5. User interface "PEP, PTT, PAT" visualization mode after 39 seconds of recording.

A "Summary" visualization window is also available in the GUI, presenting a synthesis of the most important data gathered by the device, as well as systolic blood pressure calculated from PAT and the coefficients used in the calibration.

Non-linear signal processing elements are embedded in the calculations of all these elements. Adaptive peak detectors using spline and wavelet approximations are responsible for accurate classification of the signals' parameters. Finding ECG peaks and PPG foot is rather simple when compared with I valley of the BCG. The BCG is greatly susceptible to motion artifacts, so it implements a real-time procedure for

automatic detrending, by means of wavelets [40]. Both these adaptive processes are able to attenuate the effects of baseline wavering related to muscular artifacts. Nevertheless, for HRV and BPV recordings it is important to warn the patient to be still. If the aim is to estimate the heart rate, these requirements are less important, as the system only takes three seconds to know the subject's heart rhythm.

5. RESULTS AND DISCUSSION

Five young male volunteers (age 24.7 ± 2.4 years old, weight 74.2 ± 11.8 kg (mean $\pm$ standard deviation)), without known cardiac abnormalities, were used to perform the device assessment and validation tests. After a preliminary 10 minute period with the subjects seated to relax, the data recording process started, with the volunteers being aware that they should be still during the data acquisition. The PPG sensor was placed on the left index finger and the ECG electrodes according to the Einthoven triangle on the chest. The test consisted of a continuous 10 minute recording of the BCG, ECG and PPG signals of each person, to meet the HRV standard determinations [1], and to gather an amount of data allowing extensive comparison.

A. Heart rate

The reference considered (x_{ref}) when measuring HR was the average of the three estimates. The root mean square deviations (ε_{HR}) of the estimates on each subject were computed using (7), where n is the number of heart beats of the recording, and x the signal used. Using (7) in all the signals of each recording (length of 900 ksamples), i.e., taking x = BCG, x = ECG, and x = PPG, the dispersion of ε_{HR} among the individuals produced the values of Table I.

$$\varepsilon_x = \sqrt{\frac{1}{n}\sum_{k=1}^{n}\left[x(k) - x_{ref}(k)\right]^2} \qquad (7)$$

The correlation coefficients between the HRV time estimates were obtained using the Pearson product-moment correlation coefficient, (8), where x and y represent two different signals, and μ represents the HR average of the signal.

$$\rho_{HRVx \leftrightarrow HRVy} = \frac{E\left[\left(HR_x^{-1} - \mu_x^{-1}\right)\left(HR_y^{-1} - \mu_y^{-1}\right)\right]}{\sqrt{E\left[\left(HR_x^{-1} - \mu_x^{-1}\right)^2\right]E\left[\left(HR_y^{-1} - \mu_y^{-1}\right)^2\right]}} \qquad (8)$$

Table I. Heart rate root mean square deviation results

	ECG ε_{HR} [bpm]	PPG ε_{HR} [bpm]	BCG ε_{HR} [bpm]
Subject 1	0.6369	0.6945	1.0006
Subject 2	0.3214	0.4683	0.3964
Subject 3	0.3137	0.4557	0.3836
Subject 4	0.4065	0.5082	0.6665
Subject 5	0.4392	0.5975	0.7435

Using (8) in all the signals of each recording, as in (7), the correlation coefficient, ρ, was computed for all subjects. The correlation between the signals' estimates is presented in Table II.

Table II. Heart rate variation correlation coefficient

	$\rho_{ECG\leftrightarrow PPG}$	$\rho_{BCG\leftrightarrow PPG}$	$\rho_{ECG\leftrightarrow BCG}$
Subject 1	0.9962	0.9875	0.9886
Subject 2	0.9917	0.9888	0.9947
Subject 3	0.9896	0.9862	0.9935
Subject 4	0.9948	0.9837	0.9872
Subject 5	0.9967	0.9901	0.9930

Table I and Table II results show the system's ability to correctly evaluate the heart rate and the correspondence between the signals' HRV estimates. In all the cases the heart rate presents a small absolute error, always bellow 1 bpm, and frequently bellow 0.5 bpm. All the subjects exhibit a very high correlation coefficient among all the signals' HRV. Therefore, the system provides correct estimates of heart rate. Instantaneous values and long-term trends may be obtained from ECG, PPG, or BCG without significant quality variations.

The great resemblance between the three signals' HRV estimates is illustrated in Fig.6, which depicts their power spectral density.
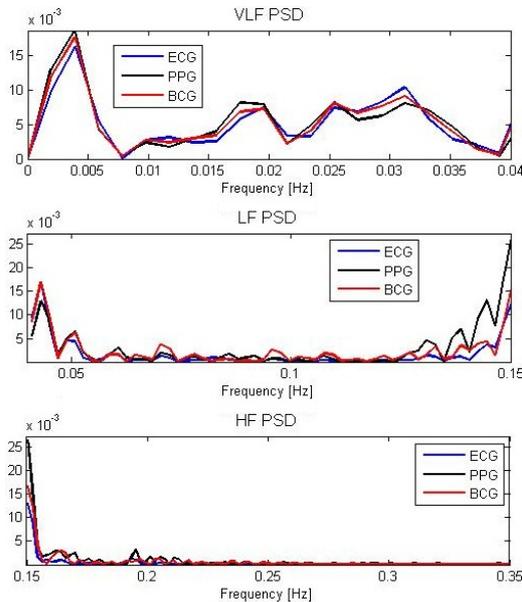

Fig.6. HRV power spectral density in V^2Hz^{-1} for one of the subjects divided in VLF, LF, and HF frequency ranges according to [1].

The HRV estimates were scrutinized in the frequency domain to evaluate their discrepancies in the ranges associated with different nervous system control actions. The customary decomposition of heart rate time series is Very Low Frequency (VLF, 0 to 0.04 Hz), Low Frequency (LF, 0.04 to 0.15 Hz) and High Frequency (HF, 0.15 to 0.50 Hz) components [2]. The High Frequency component corresponds to parasympathetic nervous system control, the Low Frequency component to sympathetic, and the VLF component to a blend of cardiovascular factors and signal processing artifacts.

Power spectrum normalized root mean square deviation (nRMSD) analysis was made in these intervals considering the average of the three estimates as reference. The results were obtained dividing the outcome of (7) by the amplitude of x_{ref} (which in this case is the difference between the minimum and the maximum of the reference's power spectral density) and are displayed in Table III.

Table III. HRV power spectrum deviations in %, in the VLF, LF, and HF frequency ranges, for all the subjects

	ECG nRMSD$_\%$	PPG nRMSD$_\%$	BCG nRMSD$_\%$
VLF	2.25±1.59	2.59±1.48	2.79±2.39
LF	7.43±5.76	7.56±3.71	9.25±11.86
HF	5.22±3.09	4.69±2.29	5.96±6.91

The results from Table III show that the ECG is the signal with most accurate results considering the reference used, with the PPG having comparable nRMSD and a tighter standard deviation. The BCG exhibits higher deviations to the average HRV estimate and with higher standard deviations. It is also noticeable that all signals have quite a small deviation in the Very Low Frequency component, with HF having twice as large deviations, and LF obtaining the less accurate estimates, both in average and in standard deviation.

B. Pulse arrival time

The correlation coefficients, ρ, between ECG to PPG delay (PAT), BCG to PPG delay (PTT), and ECG to BCG delay (PEP), removing the mean as in (8), in the 10 minutes of each recording (length of 900 ksamples) are shown in Table IV.

It can be seen that PATV estimation is well correlated to the PTTV estimation, whereas PEPV exhibits no representative relation with the PATV estimate. The best values obtained were 0.9212 and 0.5393, respectively, reinforcing this conclusion.

The PEP exhibits a near-zero correlation with the PTT which indicates, that these are quasi-independent events. This confirms that the PEP and the PTT provide complementary information on the circulatory system. The root mean square deviation of the normalized delays, nRMSD, was computed using (9), *PAT* (ECG↔PPG) and *PTT* (BCG↔PPG) denoting the delays' respective time series, resulting in nRMSD$_\%$=10.0249±2.1159.

Table IV. Cardiovascular delay variation correlation coefficient

	$\rho_{PAT\leftrightarrow PTT}$	$\rho_{PAT\leftrightarrow PEP}$	$\rho_{PEP\leftrightarrow PTT}$
Subject 1	0.7004	0.2536	-0.5128
Subject 2	0.8254	0.5393	-0.0303
Subject 3	0.8453	0.3876	-0.1650
Subject 4	0.8684	0.2677	-0.2452
Subject 5	0.9212	0.4166	0.0301

$$nRMSD\% = \sqrt{\frac{1}{n}\sum_{k=1}^{n}\left(\frac{100\times PAT(k)}{\max(PAT)-\min(PAT)}-\frac{100\times PTT(k)}{\max(PTT)-\min(PTT)}\right)^{2}} \quad (9)$$

This outcome, combined with the correlation results, makes the I valley of the BCG emerge as a possible triggering event to replace the QRS complex of the ECG, given that PTTV exhibits a strong correlation with the PATV estimates, and that heart rate and HRV results have in the BCG an alternative to the ECG with comparable results. However, if PAT calculation is substituted by the unobtrusive PTT measurement, some error is to be expected, corresponding to the influence of the PEP, which the PTT does not account for.

Analyzing the frequency content of the PATV power spectrum in terms of VLF, LF and HF, the results presented in Table V were computed.

Table V. PATV power spectrum deviations in important frequency ranges

	nRMSD%	$\rho_{PTT\leftrightarrow PAT}$			
		Subj. 2	Subj. 3	Subj. 4	Subj. 5
VLF	10.77±1.06	0.9323	0.9298	0.9025	0.9397
LF	16.77±7.33	0.8531	0.5216	0.5527	0.8923
HF	9.31±2.81	0.7324	0.6085	0.6582	0.9294

The nRMSD results presented in Table V were obtained dividing the outcome of (7) by the maximum PATV amplitude of that frequency range, in the same manner as in Table III. These results show that the two PATV have values of nRSMD about 10% in the VLF range. In the HF range a standard deviation is below 3%. In the LF range the nRMSD is larger both in average and in standard deviation.
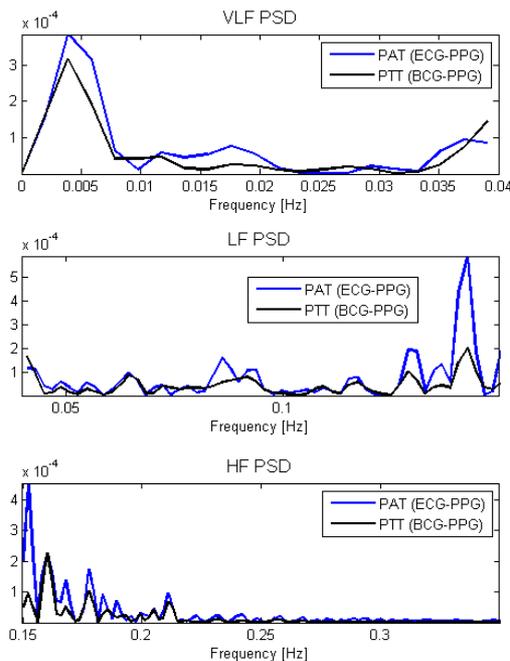

Fig.7. PATV and PTTV power spectral density in $V^{2}Hz^{-1}$ for one of the subjects, showing VLF, LF, and HF frequency ranges [1].

Regarding Table V results on Pearson product-moment correlation coefficient, it is evident that for the VLF range, the correlation between the different PATV estimates is firm. In the LF and HF ranges, although some subjects had high correlations, others have weak correlations, so LF and HF have lower average correlation with larger standard deviations. Fig.7 depicts the power spectral densities of one of the subject's PATV and PTTV, where the resemblance between these variables is visible.

The estimation of systolic blood pressure applying (1), for both PAT and PTT, is shown in Fig.8. For this recording the respective BPV is also shown. The values obtained are comparable.
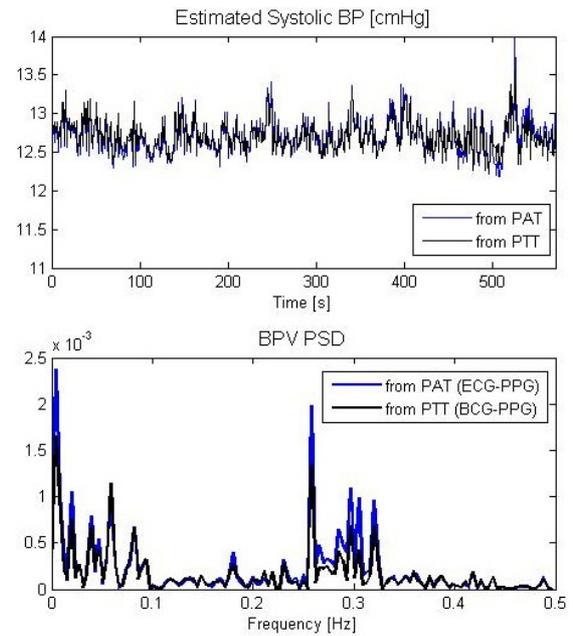

Fig.8. Systolic BP estimated from PAT and PTT (top) and the correspondent BPV power spectral density.

C. Fractal and complexity measures

The Minkowski-Bouligand dimension calculation requires a large number of values in the time series. So, it is not relevant to accompany the evolution of this parameter in the first minutes of recording. The objective is to have an estimate of its value minutes after the recording process started. From the processing of each subject's recording no significant difference was found, and all the results indicated a Minkowski-Bouligand dimension in close proximity to one.

The computational overhead of these calculations was measured by implementing the software in an Intel Core 2 Duo E6600 Dual-Core 2.4 GHz Processor, with 2 Gb RAM, running MATLAB R2007a on Windows XP. The fractal dimension of one HRV time series, obtained from a complete recording, was computed 1000 times, resulting in an average of 0.207 ms to calculate the Minkowski-Bouligand dimension of the time-series. When embedding a MATLAB script within LabVIEW 8.6, the overhead increased to 1.903 ms. Therefore, although introducing some overhead, the sparseness of this computation does not add a noteworthy delay to the system.

As the length of the HRV or PATV time series increases, the Rényi entropy increases exponentially, while Shannon entropy and Tsallis entropy increase linearly. The entropy to time series length ratio also presents a characteristic response. The results for one subject are presented in Fig.9. This type of evolution was common to all the subjects.
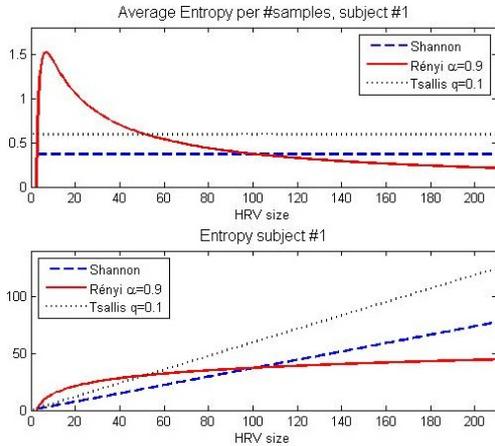

Fig.9. Total and average entropy evolution for one of the subjects.

The different subjects presented different values for the characteristic parameters of these curves. Hence it is possible to personalize the analysis, and the detection of alterations in each subject's condition. This personalization is related to the responses' amplitude and slope. Beside these parameters, timing elements are also relevant.

The difference when calculating the entropy using different signals is negligible. Considering the average entropy of the signals as reference, and adapting the formulation of (9), the nRMSD of the entropies' evolution in the five recordings was computed. The results obtained are registered in Table VI.

Table VI. Entropy deviation for different HR estimates

	ECC nRMSD$_\%$	PPG nRMSD$_\%$	BCG nRMSD$_\%$
Shannon	0.0052±0.0027	0.0041±0.0026	0.0040±0.0051
Rényi	0.0223±0.0345	0.0259±0.0105	0.0403±0.0760
Tsallis	0.0052±0.0027	0.0041±0.0026	0.0040±0.0051

These results show that all the entropies are independent of the signal used for the calculations.

Table VII presents the difference in the entropies' evolution in all the recordings when using the PTT instead of the PAT.

Table VII. Entropy deviation from PAT to PTT

	Shannon	Rényi	Tsallis
nRMSD$_\%$	1.008±2.249	0.338±0.751	0.118±0.258

From the results presented, the appropriateness of using PTT instead of PAT for estimating Rényi and Tsallis entropy of BPV is discernable. In this set of healthy subjects, the entropy has minor differences. BPV assessment from PAT provides the same result as BPV assessment from PTT. Thus, the ECG is expendable, and accurate estimation of the BPV time series entropy is achieved with PTTV, which only requires the unobtrusive BCG and PPG signals. Shannon entropy estimation is slightly coarser but still accurate.

6. CONCLUSIONS

The developed system is able to acquire and process BCG, ECG and PPG. It computes the user's heart rate from each of these signals, the corresponding pulse arrival time and pulse transit times. Evaluation of heart rate variability and PAT, PTT, and PEP variabilities is accurately done for a set of healthy and young male volunteers, allowing the estimation of blood pressure variability. Fractal dimension and three different entropies are calculated in real time, allowing the extension to non-linear methods to evaluate the cardiovascular variabilities, leading to profound and personalized assessment of heart rate evolution, and expand the knowledge on how the variabilities are progressing. These methods of analysis have verified similar results between PAT and PTT, namely PATV entropy and PTTV entropy are the same. So, whenever PTT is found sufficiently accurate for the application, only PPG and BCG are to be acquired to compute PTT, whereas PAT and ECG although providing important data, become dispensable.

Given that the calculation of these important markers of the autonomic nervous system activity is rather intrusive due to the use of the ECG signal, the possibility of using the BCG signal to replace the ECG was assessed. From HRV analysis, it was confirmed that all the signals produce comparative estimates, with reasonable differences in VLF and HF ranges, while the entropy and fractal dimension calculations are extremely consistent, regardless of the biological signal used. From delay variability analysis, it was confirmed that PTT has a strong correlation with PAT in the set of healthy subjects tested. Power spectrum density analysis of the PATV showed that the VLF component exhibits a particularly high correlation between the ECG and BCG estimates, and that both VLF and HF have moderate errors, while the LF range has larger errors.

With these results, the implemented system has proven to be accurate and trustworthy in acquiring and processing the biological signals, thus allowing the characterization of several parameters of the circulatory system. In addition to the HRV analysis, the possibility of the unobtrusive estimation of BPV, and a coarse estimate of systolic BP from PTT, was also positively assessed. However, the usage of BCG instead of ECG involves a noteworthy increase in estimation uncertainty. The patient preserves his autonomic space. The measurement does not require electrodes, but no sharp movements are allowed to minimize errors, and ensure all the recording is usable.

Future improvements of the system will aim at its connection to a database and to add artificial intelligence capabilities to it. The aim is to fuse all the data gathered by the system and compare it to the subject's history to evaluate changes in his condition. The objective will be to produce different reports to the various users, either front-end patients or medical staff.

REFERENCES

[1] Task Force of the European Society of Cardiology and the North American Society of Pacing and Electrophysiology. (1996). Heart rate variability - standards of measurement, physiological interpretation, and clinical use. *Circulation,* 93 (5), 1043-1065.

[2] Parati, G., Saul, J.P., Rienzo, M.D., Mancia, G. (1995). Spectral analysis of blood pressure and heart rate variability in evaluating cardiovascular regulation: a critical appraisal. *Hypertension,* 25, 1267-1286.

[3] Berntson, G., Cacciopo, J., Quigley, K., Fabro, V. (1994). Autonomic space and psychophysiological response. *Psychophysiology,* 31 (1), 44-61.

[4] Dawson, S.L., Manktelow, B.N., Robinson, T.G., Panerai, R.B., Potter, J.F. (2000). Which parameters of beat-to-beat blood pressure and variability best predict early outcome after acute ischemic stroke? *Stroke,* 31, 463-468.

[5] American College of Cardiology Cardiovascular Technology Assessment Committee. (1993). Heart rate variability for risk stratification of life-threatening arrhythmias. *J. Am. Coll. Cardiology,* 22, 948-950.

[6] Postolache, O., Girão, P.S., Postolache, G. (2007). New approach on cardiac autonomic control estimation based on BCG processing. In *Canadian Conference on Electrical and Computer Engineering.* Vancouver, Canada, IEEE, 876-879.

[7] Postolache, O., Postolache, G., Girão, P. (2007). New device for assessment of autonomous nervous system functioning in psychophysiology. In *IEEE International Workshop on Medical Measurements and Applications.* Warsaw, Poland, IEEE, 1-5.

[8] Pinheiro, E.C., Postolache, O. (2008). Heart rate variability virtual sensor application in blood pressure assessment system. In *Biomedical Engineering : Proceedings of the 6th IASTED International Conference.* Innsbruck, Austria, Acta Press, 79-82.

[9] Muehsltteff, J., Espina, J., Alonso, M., Aubert, X., Falck, T. (2008). Wearable body sensor network for continuous context-related pulse arrival time monitoring. In *Biomedical Engineering : Proceedings of the 6th IASTED International Conference.* Innsbruck, Austria, Acta Press, 378-383.

[10] Geddes, L.A., Voelz, M., James, S., Reiner, D. (1981). Pulse arrival time as a method of obtaining systolic and diastolic blood pressure indirectly. *Med. Biol. Eng. Comput.,* 19, 671-672.

[11] Ma, T., Zhang, Y.T. (2005). A correlation study on the variabilities in pulse transit time, blood pressure, and heart rate recorded simultaneously from healthy subjects. In *IEEE EMBS 27th Annual Conference.* Shanghai, China, IEEE, 996-999.

[12] Chen, W., Kobayashi, T., Ichikawa, S., Takeuchi, Y., Togawa, T. (2000). Continuous estimation of systolic blood pressure using the pulse arrival time and intermittent calibration. *Med. Biol. Eng. Comput.,* 38 (5), 569-574.

[13] Sugo, Y., Tanaka, R., Soma, T., Kasuya, H., Sasaki, T., Sekiguchi, T., Hosaka, H., Ochiai, R. (1999). Comparison of the relationship between blood pressure and pulse wave transit times at different sites. In *1st Joint BMES/EMBS Conference Serving Humanity, Advancing Technology.* Atlanta, USA, IEEE, 222.

[14] Steptoe, A., Smuylan, H., Gribbin, B. (1976). Pulse wave velocity and blood pressure change: calibration and applications. *Psychophysiology,* 13 (5), 488-493.

[15] Gribbin, B., Steptoe, A., Sleight, P. (1976). Pulse wave velocity as a measure of blood pressure change. *Psychophysiology,* 13 (1), 86-90.

[16] Espina, J., Falck, T., Muehlsteff, J., Aubert, X. (2006). Wireless body sensor network for continuous cuff-less blood pressure monitoring. In *3rd IEEE EMBS International Summer School and Symposium on Medical Devices and Biosensors.* Boston, USA, IEEE, 11-15.

[17] Pinheiro, E.C., Postolache, O., Girão, P. (2009). Pulse arrival time and ballistocardiogram application to blood pressure variability estimation. In *IEEE International Workshop on Medical Measurement and Applications.* Cetraro, Italy, IEEE, 132-135.

[18] Kiu, Y., Poon, C., Zhang, Y. (2008). A hydrostatic calibration method for the design of wearable PAT-based blood pressure monitoring devices. In *IEEE EMBS 30th Annual Conference.* Vancouver, Canada, IEEE, 1308-1310.

[19] Skinner, J., Anchin, J., Weiss, D. (2008). Nonlinear analysis of the heartbeats in public patient ECGs using an automated PD2i algorithm for risk stratification of arrhythmic death. *Ther. Clin. Risk Manag.,* 4 (2), 549-557.

[20] Yeragani, V.K., Srinivasan, K., Vempati, S., Pohl, R., Balon, R. (1993). Fractal dimension of heart rate time series: an effective measure of autonomic function. *J. Appl. Phys.,* 75 (6), 2429-2438.

[21] Skinner, J., Pratt, C., Vybiral, T. (1993). A reduction in the correlation dimension of heartbeat intervals precedes imminent ventricular fibrillation in human subjects. *Am. Heart J.,* 125 (3), 731-743.

[22] Vybiral, T., Skinner, J. (1993). The point correlation dimension of R-R Intervals predicts sudden cardiac death among high-risk patients. In *Computers in Cardiology,* London, UK, IEEE, 257-260.

[23] Storella, R., Wood, H., Mills, K., Kanters, J., Højgaard, M., Holstein-Rathlou, N. (1998). Approximate entropy and point correlation dimension of heart rate variability in healthy subjects. *Integr. Physiol. Behav. Sci.,* 33 (4), 315-320.

[24] Yeragani, V., Sobolewski, E., Jampala, V., Kay, J., Yeragani, S., Igel, G. (1998). Fractal dimension and approximate entropy of heart period and heart rate:

awake versus sleep differences and methodological issues. *Clin. Sci.,* 95 (3), 295-301.

[25] Perkiömäki, J., Mäkikallio, T., Huikuri, H. (2005). Fractal and complexity measures of heart rate variability. *Clin. Exp. Hypertens.,* 27 (2-3), 149-158.

[26] Richman, J., Moorman, J. (2000). Physiological time-series analysis using approximate entropy and sample entropy. *Am. J. Physiol. Heart Circ. Physiol.,* 278 (6), 2039-2049.

[27] Rosso, O., Martin, M., Figliola, A., Keller, K., Plastino, A. (2006). EEG analysis using wavelet-based information tools. *J. Neurosci. Methods,* 153 (2), 163-182.

[28] Lunak, D.R., Bryngelson, R.S. (2006). *Noninvasive Blood Pressure Monitor Having Automatic High Motion Tolerance.* U.S. Patent No. 7,052,465. Washington, D.C.: U.S. Patent and Trademark Office.

[29] Foo, J.Y.A., Lim, C.S. (2006). Pulse transit time as an indirect marker for variations in cardiovascular related reactivity. *Technol. Health Care,* 14 (2), 97-108.

[30] Muehlsteff, J., Aubert, X., Schuett, M. (2006). Cuffless estimation of systolic blood pressure for short effort bicycle tests: the prominent role of the pre-ejection period. In *IEEE EMBS 28th Annual Conference.* New York, USA, IEEE, 5088-5092.

[31] Payne, R.A., Symeonides, C.N., Webb, D.J., Maxwell, S.R.J. (2006). Pulse transit time measured from the ECG: an unreliable marker of beat-to-beat blood pressure. *J. Appl. Physiol.,* 100, 136-141.

[32] Pinheiro, E.C., Postolache, O., Girão, P. (2010). Theory and developments in an unobtrusive cardiovascular system representation: Ballistocardiography. *Open Biomed. Engin. J.,* 4, 201-216.

[33] Schroeder, M. (1991). *Fractals, Chaos, Power Laws: Minutes from an Infinite Paradise.* New York, USA: W.H. Freeman.

[34] Costa, M., Goldberg, A.L., Peng, C.K. (2002). Multiscale entropy analysis of complex physiologic time series. *Phys. Rev. Lett.,* 89 (6), 021906.

[35] Pincus, S.M. (1991). Approximate entropy as a measure of system complexity. *Proc. Natl. Acad. Sci. USA,* 88, 2297-2301.

[36] Richman, J.S., Moorman, J.R. (2000). Physiological time-series analysis using approximate entropy and sample entropy. *Am. J. Physiol. Heart Circ. Physiol.,* 278 (6), 2039-2049.

[37] Goldberger, A.L., Peng, C.K., Lipsitz, L.A. (2002). What is physiologic complexity and how does it change with aging and disease? *Neurobiol. Aging,* 23 (1), 23–26.

[38] Lekkala, J., Paajane, M. (1999). EMFi – new electret material for sensors and actuators. In *10th IEEE International Symposium on Electrets.* Delphi, Greece, IEEE, 743-746.

[39] Strong, P. (1970). *Biophysical Measurements.* Beaverton, USA: Tektronix.

[40] Pinheiro, E.C., Postolache, O., Girão, P. (2010). Automatic wavelet detrending benefits to the analysis of cardiac signals acquired in a moving wheelchair. In *32nd Annual International Conference of the IEEE EMBS.* Buenos Aires, Argentina, IEEE, 602-605.